

Flourishing chemosynthetic life at the greatest depths of hadal trenches

<https://doi.org/10.1038/s41586-025-09317-z>

Received: 31 December 2024

Accepted: 23 June 2025

Published online: 30 July 2025

Open access

 Check for updates

Xiaotong Peng^{1,7}, Mengran Du^{1,7}✉, Andrey Gebruk², Shuangquan Liu¹, Zhaoming Gao¹, Ronnie N. Glud³, Peng Zhou¹, Ruoheng Wang¹, Ashley A. Rowden^{4,5}, Gennady M. Kamenev⁶, Anastassya S. Maiorova⁶, Dominic Papineau¹, Shun Chen¹, Jinwei Gao¹, Helu Liu¹, Yuan He¹, Inna L. Alalykina⁶, Igor Yu. Dolmatov⁶, Hanyu Zhang¹, Xuegong Li¹, Marina V. Malyutina⁶, Shamik Dasgupta¹, Anastasiia A. Saulenko⁶, Vladimir A. Shilov⁶, Shuting Liu¹, Tongtong Xie¹, Yuangao Qu¹, Xikun Song¹, Haibin Zhang¹, Hao Liu¹, Weijia Zhang¹, Xiaoxia Huang¹, Hongzhou Xu¹, Wenjing Xu¹, Vladimir V. Mordukhovich^{6,7}✉ & Andrey V. Adrianov⁶

Hadal trenches, some of the Earth's least explored and understood environments, have long been proposed to harbour chemosynthesis-based communities^{1,2}. Despite increasing attention, actual documentation of such communities has been exceptionally rare^{3,4}. Here we report the discovery of the deepest and the most extensive chemosynthesis-based communities known to exist on Earth during an expedition to the Kuril–Kamchatka Trench and the western Aleutian Trench using the manned submersible *Fendouzhe*. The communities dominated by siboglinid Polychaeta and Bivalvia span a distance of 2,500 km at depths from 5,800 m to 9,533 m. These communities are sustained by hydrogen sulfide-rich and methane-rich fluids that are transported along faults traversing deep sediment layers in trenches, where methane is produced microbially from deposited organic matter, as indicated by isotopic analysis. Given geological similarities with other hadal trenches, such chemosynthesis-based communities might be more widespread than previously anticipated. These findings challenge current models of life at extreme limits and carbon cycling in the deep ocean.

Chemosynthesis-based communities represent a remarkable example of life's ability to adapt and thrive in some of the most extreme conditions on Earth^{5–8}. Since the initial discovery of these communities at hydrothermal vents⁹, the detection of chemosynthesis-based communities at cold seeps, supporting highly diverse and abundant chemosymbiotic biota^{1,3–8}, has increased and expanded our understanding of deep-sea ecological systems and the biogeochemical processes that underpin them. The communities, typically dominated by Bivalvia and Siboglinidae, and sustained by microbial chemosynthesis, are confined to areas where fluids rich in hydrogen sulfide and/or methane are released through geological fractures^{6,7}.

Despite being found on passive and active margins across a wide range of ocean depths^{5–8}, cold-seep communities have remained largely unexplored in hadal trenches with depths exceeding 6,000 m. Only two small seep communities at hadal depths have been discovered by submersible and remotely operated vehicle, one dominated by vesicomyid clams at nearly 6,437 m depth and another dominated by thyasirid clams at 7,326–7,434 m in the Japan Trench^{3,4,10}. In addition, probable chemosynthetic mats have been observed at a depth of 10,677 m at the bottom of the Mariana Trench¹¹; however, they are not associated with any seep animal communities. The biogeographical distribution of chemosynthesis-based communities in the deepest parts of the world's oceans, their potential roles in shaping the deep-sea ecosystem

and the mechanisms behind the formation of methane seeps at such great depths remain elusive.

The Kuril–Kamchatka Trench and the Aleutian Trench are formed by the tectonic interactions between the Pacific Plate and the North American Plate, and meet at the Kamchatka Aleutian Transition connection¹². This area is geologically highly active with many seismically and volcanically active sites. The Kuril–Kamchatka Trench is formed by the northwestward subduction of the Pacific Plate beneath the Okhotsk Plate and extends around 2,100 km from Hokkaido in the south to Kamchatka Peninsula in the north¹³. The maximum depth of the trench bottom reaches 9,578 m, based on our submersible conductivity–temperature–depth data. Previous research conducted by expeditions aboard research vessel (RV) *Vityaz* and RV *Sonne* in the Kuril–Kamchatka Trench shows that the trench is characterized by predominantly heterotrophic benthic fauna^{14,15}. However, some specimens of chemosymbiotic taxa^{15,16}, in particular frenulate siboglinids, were also recovered using a trawl, indicating that methane seeps may exist on the trench bottom. The Aleutian Trench is about 2,900 km long, extends from the Alaska and Kenai peninsulas in North America to Kamchatka¹³ and marks a boundary where the Pacific Plate has been subducting northwestwards beneath the Bering Sea Plate. Both trenches underlie a highly productive boreal region of the North Pacific Ocean and are characterized by distinct spring blooms and high annual primary production¹⁷.

¹State Key Laboratory of Deep-sea Science and Intelligence Technology, Institute of Deep-sea Science and Engineering, Chinese Academy of Sciences, Sanya, China. ²Shirshov Institute of Oceanology, Russian Academy of Sciences, Moscow, Russia. ³Department of Biology, Danish Center for Hadal Research, University of Southern Denmark, Odense, Denmark. ⁴National Institute of Water and Atmospheric Research, Wellington, New Zealand. ⁵School of Biological Sciences, Victoria University of Wellington, Wellington, New Zealand. ⁶A.V. Zhirmunsky National Scientific Center of Marine Biology, Russian Academy of Sciences, Vladivostok, Russia. ⁷These authors contributed equally: Xiaotong Peng, Mengran Du. ✉e-mail: mdu@idsse.ac.cn; vvmora@mail.ru

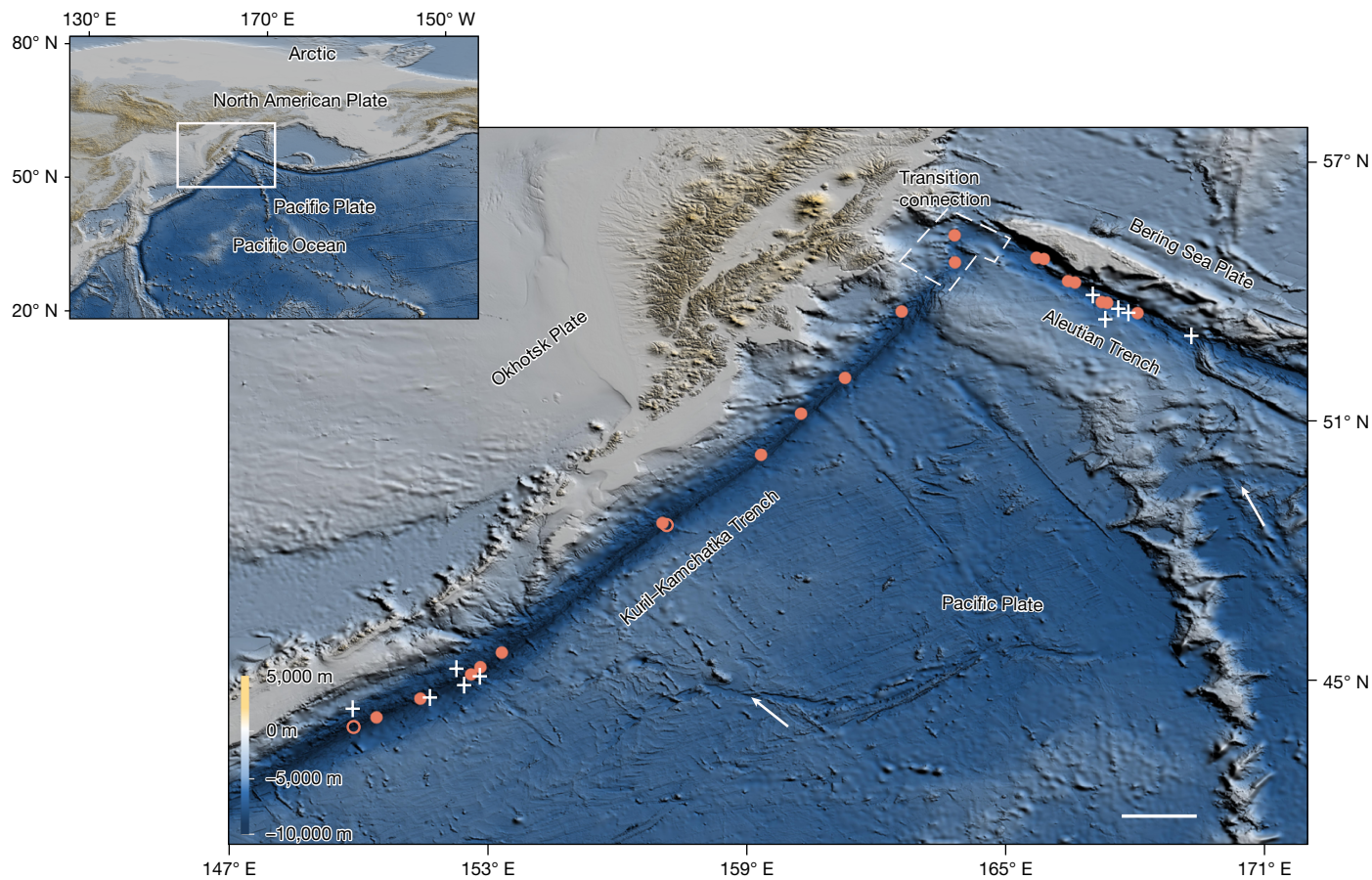


Fig. 1 | Map showing the Kuril–Kamchatka Trench and western Aleutian Trench. The study area, situated in the northwest Pacific, is demarcated by a white rectangle in the inset. Orange dots represent dive sites where chemosynthesis-based communities were observed and sampled and crosses indicate dive sites lacking such communities. Open orange circles delineate potential seep sites characterized by black sediments. White arrows illustrate the direction of subduction for the Pacific Plate beneath the Okhotsk Plate

and the Bering Sea Plate. The dashed white lines indicate the transitional connection zones between the Kuril–Kamchatka Trench and the Aleutian Trench. Bathymetric data were acquired using the KM-EM122 multi-beam bathymetric system during the research expedition. Scale bar, 200 km. Credit: map created using Global Mapper 14 software, with background data sourced from GeoMapApp (<http://www.geomapapp.org>), under a CC BY 4.0 licence.

Chemosynthetic community distribution and diversity

Investigations of the trench bottom of the Kuril–Kamchatka Trench and the western Aleutian Trench from 8 July to 17 August 2024, using RV *Tansuoyihao* with the full-ocean-depth manned submersible *Fendouzhe* capable of reaching the deepest part of the ocean at nearly 11,000 m, resulted in the discovery of widespread cold-seep chemosynthesis-based communities in both trenches (Fig. 1). During dive FDZ 271 in the Kuril–Kamchatka Trench, we first encountered dense chemosynthetic communities dominated by frenulate siboglinids at a depth of 9,533 m, situated atop black muds at the boundary between the trench bottom and the basement of the accretionary prism. This boundary corresponds to the outcrop of a geological normal fault, a feature formed by bending of the incoming plate, as indicated by regional seismic data¹⁸. We have designated this seep site as The Deepest because of its unparalleled depth, marking it as the deepest known seepage location discovered so far (Fig. 2a). Subsequent to this initial discovery, we executed a comprehensive series of 23 dives in geologically analogous settings to determine the spatial distribution, scale and biodiversity of the chemosynthetic communities inhabiting the trench floors. During 19 of these dives (Supplementary Table 1), we observed, recorded and sampled chemosynthesis-based communities, revealing their proliferation in a distinct zone along the basement of the accretionary prism. This zone stretches 2,500 km along the bottom of the

trenches, representing a notable ecological feature of these two hadal trenches that has not been recognized or reported despite previous sediment and fauna investigations in these areas.

The species composition and structure of chemosynthesis-based communities in the Kuril–Kamchatka Trench, with depths ranging from nearly 7,000 m to 9,533 m, is distinct from those observed in the Kamchatka Aleutian Transition and the western Aleutian Trench where depths are predominantly less than 7,000 m. In the Kuril–Kamchatka Trench, most communities are dominated by frenulate siboglinids (Extended Data Fig. 1). The composition of siboglinid species among communities in the Kuril–Kamchatka Trench seems to differ considerably. The most abundant species are representatives of *Lamellisabella*, *Polybrachia*, *Spirobrachia* and *Zenkevitchiana*. A notable discovery in the central Kuril–Kamchatka Trench at a depth of 9,120 m (dive FDZ 274) is the Wintersweet Valley site, which is predominantly inhabited by two species of frenulate siboglinids (*Lamellisabella* and *Polybrachia*) (Fig. 2b). These frenulate siboglinids were found in great abundance along a substantial portion of a seep field, around 2 km in length, which was explored during a single dive. The colonies consist of thousands of individuals with tubes extending out of the sediment. Associated with the frenulate siboglinids is a suite of species obligate to this particular habitat, including tube-dwelling polychaetes *Terebelliformia* and numerous *Gastropoda* that settled on the siboglinid tubes, as well as a variety of heterotrophic benthic fauna including free-moving polychaetes *Macelicephalooides*, crinoids *Bathycriinus*, holothurians *Elpidia hansenii* and amphipods cf. *Princaxelia*.

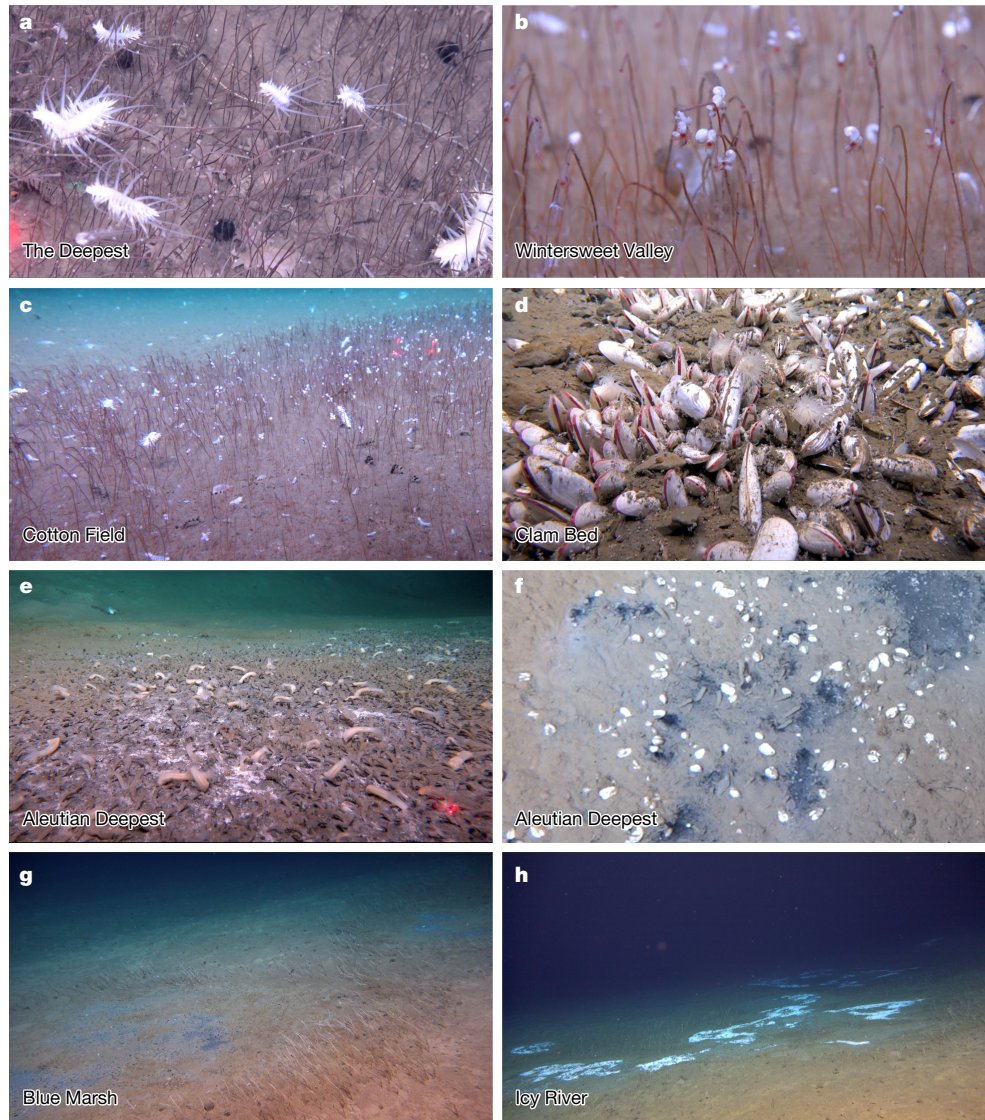


Fig. 2 | Representative fauna of cold-seep sites in the Kuril–Kamchatka Trench and western Aleutian Trench. **a**, Free-moving polychaetes *Macellicephaloides grandicirra* (white; reaching 6.5 cm in size) navigate among dense colonies of frenulate siboglinids, with tubes 20–30 cm in length and approximately 1 mm in diameter, at 9,532 m at The Deepest. **b**, Clusters of frenulate siboglinids extending red haemoglobin-filled tentacles, with small Gastropoda (white spots) on tops of the tubes near the tentacles, at 9,320 m at Wintersweet Valley. **c**, Tightly packed frenulate siboglinids are home to abundant free-moving polychaetes *M. grandicirra* (white) at 9,332 m at Cotton Field. **d**, Dense aggregation of vesicomyid bivalves *A. phaseoliformis* (reaching 23 cm in size) in the sediment, with approximately 6–8 cm of valves exposed and often hosting Actiniaria, at 5,743 m at Clam Bed. **e**, Tube-dwelling

polychaetes *Anobothrus* sp. and Actiniaria are dominant at 6,870 m at Aleutian Deepest, with spots of white microbial mats. **f**, Dense aggregation of vesicomyid bivalves *I. fossajaponicum* (reaching 3 cm in size) associated with black sediments and accompanied by tube-dwelling polychaetes *Anobothrus* sp. at 6,928 m at Aleutian Deepest. **g**, Dark blue muds surrounded by clusters of frenulate siboglinids, mark methane seeps at 6,800 m at Blue Marsh. **h**, Large patches of white, snow-like microbial mats stretch tens of metres, accompanied by frenulate siboglinid tubeworms at 6,700 m at Icy River. The images were taken by the manned submersible equipped with a high-definition camera system. The name of each cold seep indicated in the lower left corner. The distance between laser beams is 10 cm. An expanded showcase of cold-seep fauna is given in Supplementary Video 1.

In addition, two other large cold-seep fields, the Dead Valley and Cotton Field sites, were observed at depths of 9,522 and 9,566 m during dive FDZ 275. These fields are located roughly 120 km southwest of Wintersweet Field and extend at least 2.2 km along the 9,520 m contour line. In Dead Valley, dense clusters of frenulate siboglinids occur, with tubes covered by white flocculent material and lying almost horizontally (Extended Data Fig. 2). Siboglinids seem to be dead, suggesting cessation of fluid activity in this part of the field. By contrast, Cotton Field (Fig. 2c), situated 50 m southwest of Dead Valley, supports dense populations of living frenulate siboglinids in association with numerous free-moving polychaetes (Macellicephalinae) and Gastropoda. It is noteworthy that frenulate siboglinids were encountered in nine

of eleven dives conducted at the base of the accretionary prisms in the Kuril–Kamchatka Trench, albeit with varying densities of occurrence. During dive FDZ 278, frenulate siboglinids with a relatively high abundance of thyasirid bivalves (*Tartarothyasira* cf. *hadalis*) and tube-dwelling polychaetes (*Anobothrus* sp.) were discovered at a depth of 8,764 m. *Tartarothyasira hadalis* (initially described as *Maorithyas hadalis*¹⁰) has been documented in the hadal zone of the Japan Trench at a depth of 7,326–7,434 m (refs. 3,11). The presence of these chemosymbiotic bivalves in the Kuril–Kamchatka Trench marks the deepest occurrence of such organisms ever discovered in hadal zones.

In contrast to the Kuril–Kamchatka Trench, the chemosynthesis-based communities located in the Kamchatka Aleutian Transition are

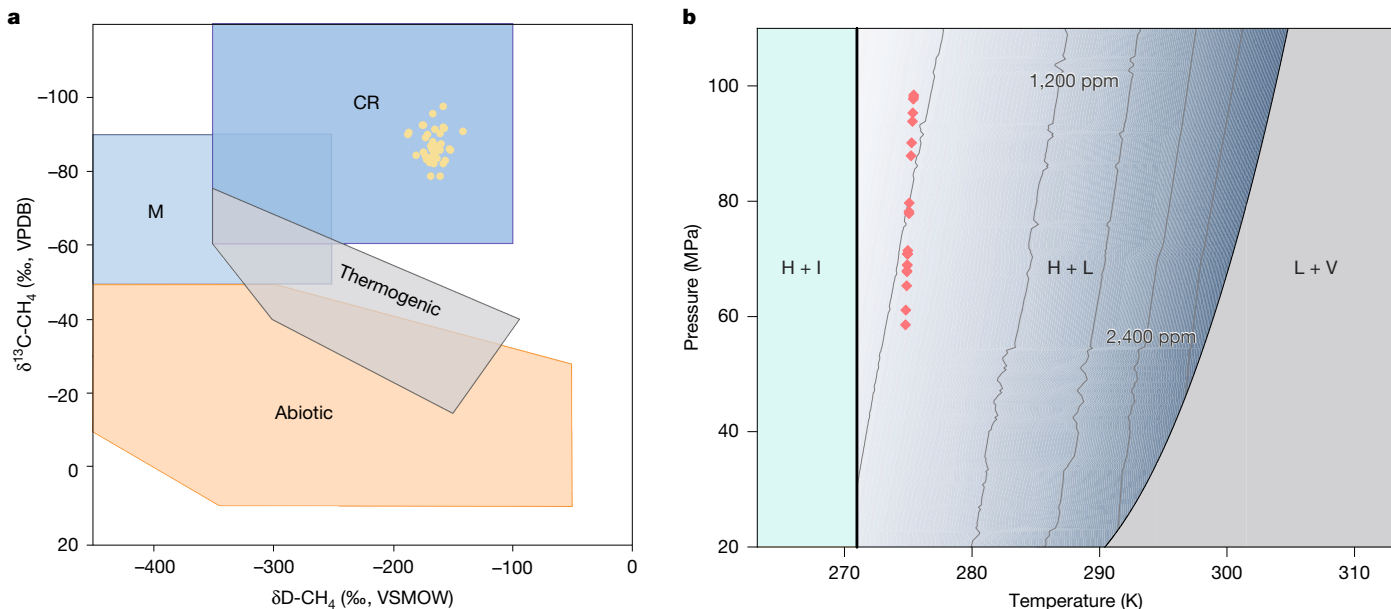


Fig. 3 | Origins and phases of methane in hadal cold seeps. **a**, $\delta^{13}\text{C-CH}_4$ (‰, VPDB) and $\delta\text{D-CH}_4$ (‰, VSMOW) diagram classifying the source of methane. The base diagram is adapted from previous studies^{25,26,28}, which used field measurements of stable carbon and hydrogen isotopes of methane (CH_4) from diverse sedimentary environments to distinguish between different types of microbial and thermogenic methanogenesis. Yellow dots in the CO_2 reduction (CR) category represent data from the methane samples analysed

in this study. **b**, Schematic phase diagram of methane hydrate–sea water system. Solid black lines represent the phase boundaries between $\text{H}+\text{I}$ – $\text{H}+\text{L}$ and $\text{H}+\text{L}$ – $\text{L}+\text{V}$; the shaded (grey blue) $\text{H}+\text{L}$ phase zone and grey lines therein indicate the methane hydrate solubilities in sea water (mCH_4 , in ppm). Red diamonds represent the temperature and pressure conditions at stations where seeps are present. $\text{H}+\text{I}$, methane hydrate + ice; $\text{H}+\text{L}$, methane hydrate + liquid; $\text{L}+\text{V}$, liquid + vapour; M, methyl-based methanogenesis.

characterized by a high abundance of two species of chemosymbiotic vesicomyid clams *Abyssogena phaseoliformis* and *Isorropodon fossajaponicum* (Extended Data Table 1 and Extended Data Fig. 3). Fields of siboglinids and clusters of bivalves in the Kamchatka Aleutian Transition were located next to each other, but did not overlap. During dive FDZ 284, dense aggregations of bivalves were initially identified in muddy sediments at a depth of 5,988 m. The communities in this field are largely dominated by *I. fossajaponicum* and tube-dwelling ampharetid polychaetes (*Anobothrus* sp.). On the subsequent dive, FDZ 297, an expansive seep field termed Clam Bed (Fig. 2d) was discovered, extending roughly 2 km along a steep fault at a depth of 5,800 m. The dominant species in this community is *A. phaseoliformis*. In addition to clams, the seep field supports a diverse array of fauna, including gastropods Peltospiridae and Provanidae, tube-dwelling polychaetes Ampharetidae and Maldanidae, free-moving polychaetes Polynoidae and Dorvilleidae, amphipods cf. *Abyssododecas* and actiniarians Sagartiidae. Similar *A. phaseoliformis* dominated communities have previously been described for the Japan Trench and the eastern Aleutian Trench^{19,20}.

The cold-seep communities in the western Aleutian Trench are dominated by Bivalvia, Siboglinidae or Ampharetidae. During dives FDZ 285 and FDZ 296, we documented the presence of thyasirid (*Tartarothyasira* cf. *hadalis* and *Axinus* sp.) and vesicomyid (*I. fossajaponicum*) bivalve aggregations (Extended Data Table 1), as well as tube-dwelling polychaetes *Anobothrus* sp. (Fig. 2e,f), distributed discontinuously along a 5-km stretch of a subducting normal fault between depths of 6,900 and 6,930 m. In addition, during dive FDZ 286, a large field of *Tartarothyasira* cf. *hadalis* more than 500 m across was observed at a depth of 6,756 m (Extended Data Fig. 2). Frenulate siboglinids are primarily located around the periphery of areas with aggregations of bivalves. During dives FDZ 294 and FDZ 295, a seep field designated as Blue Marsh (Fig. 2g) extending over at least 2 km, was discovered at a depth of 6,635 m. The central regions of these seeps are commonly dominated by tube-dwelling Ampharetidae, whereas the margins are predominantly inhabited by frenulate siboglinids, *Polybrachia*, *Spirobrachia* and *Zenkevitchiana*. Furthermore, a seep field named Icy River

(Fig. 2h) was noted east of the Blue Marsh field at a depth of 6,630 m. This field is characterized by white microbial mats surrounded by frenulate siboglinids. In comparison with the Kuril–Kamchatka Trench, the abundance of bivalves and tube-dwelling polychaetes in the western Aleutian Trench is notably higher.

The seep communities identified in this study, akin to those documented in the hadal zone and at shallower depths^{3,4,20–22}, are distinguished by their exceptionally high abundance and density of specialized species. We found maximum densities of up to $5,813 \pm 1,335$ (mean \pm s.d.) Siboglinidae and 293 ± 69 Bivalvia per square metre in two trenches (Supplementary Table 1). The composition and structure of the investigated communities exhibit a marked patchiness across various spatial scales. This variability is observed not only in individual trenches and across depth ranges, but also between different trenches. Furthermore, certain species are distributed across a broad latitudinal and bathymetric gradient. The consistent presence of the same chemosymbiotic species across the Japan, Kuril–Kamchatka and Aleutian trenches suggests the presence of a connected system of reducing habitats in the hadal zone of the northern Pacific. Connections among the trench-hosted seep communities may extend even farther south to the Japan and Mariana trenches, as suggested by the presence of similar looking clam taxa^{20–22}.

Pore-water and carbonate geochemistry

The molecular and isotopic compositions of gases associated with cold seeps in the seep sediments provide compelling evidence for a microbial origin of methane (Extended Data Table 2). Analysis of hydrocarbon in head gases and sediments of pushcores showed that methane constitutes 100% of the total hydrocarbons, suggesting a microbial origin for the methane^{23,24}. Analysis of carbon (C) and deuterium (D) stable isotope showed that methane samples exhibited $\delta^{13}\text{C}_{\text{VPDB}}$ (Vienna Pee Dee Belemnite) values ranging from $-78.1\text{\textperthousand}$ to $-95.7\text{\textperthousand}$ and $\delta\text{D}_{\text{VSMOW}}$ (Vienna Standard Mean Ocean Water) values ranging from $-142.2\text{\textperthousand}$ to $-188.8\text{\textperthousand}$. These findings further indicate that the methane is derived

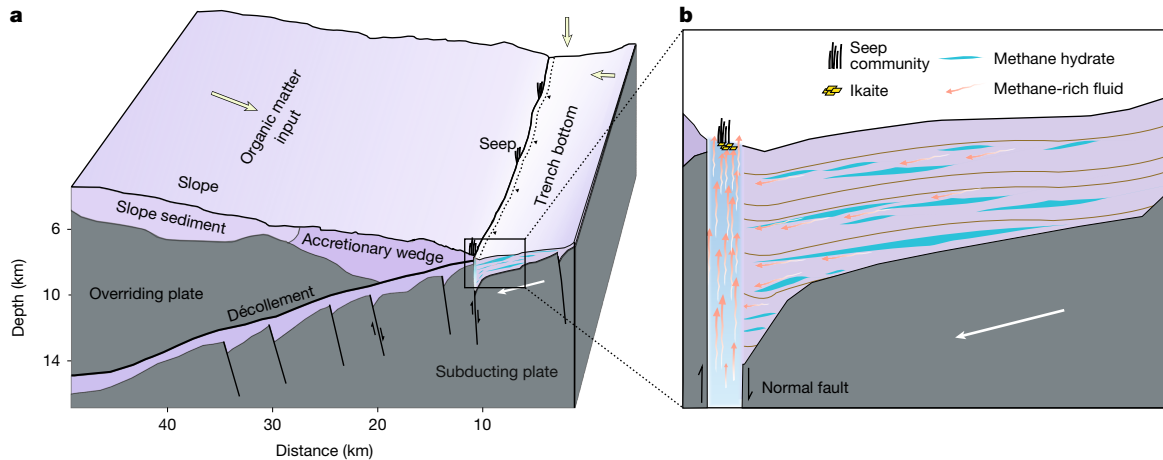


Fig. 4 | Formation of hadal trench cold seeps. **a**, Schematic geological model presenting the cross-section view of the subducting plate and the overriding plate along the trench, as indicated by seismic survey data¹⁸ from these areas. The light green arrows depict the migration of organic matter into the trench, encompassing both downward and lateral movements. The white arrow denotes the direction of subduction, and the dashed line signifies the trench axis, which is nearly parallel to the striped zone of cold seeps. Black triangles point to the trench's axis. Note the prevalence of normal faults developed in the

subducting plate. **b**, Detailed view of the area outlined by the black rectangle in **a** showing the formation of gas hydrates in deep sediment layers. Methane-rich fluids migrate horizontally towards the accretionary wedge as a result of the compression forces associated with subduction. Normal faults at the leading edge of the accretionary wedge create a pathway that facilitates the upward migration of seep fluids. Figure created using previously published location data¹⁸ of subducting bending faults.

from microbial carbonate reduction rather than from methyl-based methanogenesis^{25–28} (Fig. 3a). These geochemical data collectively indicate that the methane present in the seep sediments is the result of microbial reduction of CO₂ derived from sedimentary organic matter.

The sediments associated with cold seeps are typically dark grey to black, coloration attributed to the high iron sulfide content present in the sediment matrix. Upon retrieval, sediment cores from these seeps exhibited a distinct hydrogen sulfide odour. The vertical profiles of methane, ammonia (NH₄⁺), dissolved organic carbon, dissolved inorganic carbon (DIC), δ¹³C-DIC, sulfate (SO₄²⁻), hydrogen sulfide and salinity in two pushcores showed typical distribution patterns associated with cold-seep environments (Extended Data Fig. 4). These patterns indicate the processes of anaerobic methane oxidation coupled with sulfate reduction^{5,29,30}, organic matter diagenesis^{5,30} and hydrate decomposition³¹. In addition, metastable hexahydrate calcium carbonate (ikaite, CaCO₃·6H₂O), with clusters of euhedral spear-like crystals (Extended Data Fig. 5), are found in association with the black sediments of cold seeps. Ikaite δ¹³C values range from -17.29‰ to -26.89‰ (Extended Data Table 3), suggesting that they are probably authigenic precipitates from CO₂³² supplied from the early diagenetic decomposition of sedimentary organic matter³², preceding microbial methane oxidation.

The modelling of methane phases under hadal zone conditions (Fig. 3b) indicates that at all observed seep sites at depths ranging from 5,662 m to 9,533 m, methane occurs in a dissolved form in pore water and as hydrate, with the absence of a vapour phase. This finding aligns with in situ observations conducted by submersible, which have noted the absence of bubbling and any associated gas phase during dives. Methane concentrations measured in the headspace of sediment pushcore reached 118,882 ppm, substantially exceeding the methane solubility in equilibrium with hydrate at these depths (545 ppm at 9,500 m). Calculation of the hydrate stability zone (Extended Data Fig. 6) indicates the potential presence of hydrates at these profound depths in sedimentary layers. A focused coring and drilling campaign is needed to revisit these seeps to validate this hypothesis.

Formation of hadal cold seeps

The formation processes of cold seeps on trench bottoms differ markedly from those located on accretionary prisms at shallower depths.

Cold seeps on accretionary prisms are characterized by the ejection of fluids through thrust faults^{33–35}, with these fluids originating from subducted sediments and migrating upwards over distances often exceeding 1,000 m (ref. 36). By contrast, this study indicates that the fluids associated with trench-bottom seeps are sourced from trench sediments that have not been subducted. This hypothesis is bolstered by the composition of the fluids, primarily biogenic methane—typically produced through microbial carbonate reduction a few to several hundred metres beneath the seabed³⁷. We propose that these fluids from the deep sediment layers of the trench migrate upwards along bending-related faults or other major fractures that occur at the leading edge of the accretionary prisms.

Figure 4 illustrates a geological model of cold-seep formation in the Kuril–Kamchatka and Aleutian trenches. In these trenches, the V-shaped topography serves as a natural trap, facilitating the rapid accumulation of substantial quantities of organic matter on the trench bottom^{38,39}. This organic matter is introduced from the highly productive ocean surface where phytoplanktonic blooms frequently occur and from the trench slope by means of gravity flows triggered by earthquakes and landslides^{40,41}. Under the anoxic conditions prevalent in the deep sediment layers, microbial reduction of carbon dioxide derived from sedimentary organic material can sustain methanogenesis^{25–28}. We argue that, over time, this methane accumulates beneath impermeable sediment layers in the form of dissolved methane fluid and methane hydrate. The compression forces associated with incoming plate subduction⁴² then facilitate the lateral migration of methane fluids in the deep sediment layers at the trench bottom, directing them towards the accretionary prism. Ultimately, methane fluids migrate upwards through large fault zones (for instance, bending-related normal faults) that occur at the basement of the accretionary prism. Upon reaching the sea floor, methane fluids escape as a hadal cold seep and support the observed chemosynthesis-based ecosystems.

Implications

Although hadal seeps have been documented before, the depths probed here, coupled with the thriving communities discovered and distribution ranges observed, significantly expand the known habitat, depth and biogeographical distributions for a great many species.

Article

Moreover, studies of organisms thriving in these communities can provide clues about physiological boundaries, adaptive strategies and previously unknown animal–microbe interactions shaped by high-pressure conditions¹. Our findings also challenge the traditional perspective on the energy sources sustaining hadal fauna, which were predominantly believed to be derived from surface-derived particulate organic matter and carrion fall⁴³. The widespread occurrence of chemosynthesis-based communities suggests an underappreciated role of chemical energy in shaping the hadal ecosystem. The co-existence of chemosynthesis-based organisms with a substantial number of heterotrophic benthic fauna, such as Actiniaria, Echiura, Holothuroidea and Amphipoda (Extended Data Fig. 7), suggests that methane seep production in the trench extends its influence to the broader benthic community⁴⁴. If such a trophic subsidy for heterotrophic benthic fauna is demonstrated and quantified by follow-up research, this study would have served to highlight a previously unrecognized contribution of chemosynthetic processes to the overall functioning of hadal ecosystems.

The detection of anomalously high methane concentrations and the potential for gas hydrate formation in the hadal zone provide new insights into deep carbon cycling. The widespread methane-rich environments in two hadal trenches, where microbial reduction of CO₂ from sedimentary organic matter presumably results in methane production, suggest a vibrant and active microbial community in the hadal sediments. This indicates that the deep-subsurface biosphere may exert a more important influence on biogeochemical processes in subduction zones, representing a previously unrecognized energy supply^{45,46}. The accumulation of methane in sedimentary layers generated by this deep-subsurface biosphere could potentially sequester considerable amounts of sedimentary organic carbon, suggesting a portion of subducting organic carbon can be stored in the trench sediments in a form of methane for prolonged geological time, rather than being subducted to the deep lithosphere. It remains unknown whether the current findings can be extrapolated to other trench systems, but given the geological similarities hadal methane reservoirs may be more widespread, irrespective of the presence of fault zones that could serve as conduits for the release of methane-rich fluids. This hypothesis is supported by the recovery of gas hydrates from drilling sediments in the Middle America Trench⁴⁷ and the Peru–Chile Trench at depths surpassing 5,000 m (ref. 48), and the presence of similar seep communities in the Japan Trench^{3,4}. These findings underscore the complex nature of carbon cycling in the deep sea and highlight the critical need to integrate hadal processes into global carbon models^{49,50} to improve the accuracy of predictions about carbon dynamics and climate change responses on geological timescale. Furthermore, the potential presence of methane hydrates at great depths in hadal trenches may enhance global inventory of methane gas hydrate resources.

Online content

Any methods, additional references, Nature Portfolio reporting summaries, source data, extended data, supplementary information, acknowledgements, peer review information; details of author contributions and competing interests; and statements of data and code availability are available at <https://doi.org/10.1038/s41586-025-09317-z>.

1. Boulègue, J., Benedetti, E. L., Dron, D., Mariotti, A. & Létolle, R. Geochemical and biogeochemical observations on the biological communities associated with fluid venting in Nankai Trough and Japan Trench subduction zones. *Earth Planet. Sci. Lett.* **83**, 343–355 (1987).
2. Blankenship-Williams, L. E. & Levin, L. A. Living deep: a synopsis of hadal trench ecology. *Mar. Technol. Soc. J.* **43**, 137–143 (2016).
3. Fujikura, K. et al. The deepest chemosynthesis-based community yet discovered from the hadal zone, 7326 m deep, in the Japan Trench. *Mar. Ecol. Prog. Ser.* **190**, 17–26 (1999).
4. Ogawa, Y., Fujioka, K., Fujikura, K. & Iwabuchi, Y. En echelon patterns of Calyptogena colonies in the Japan Trench. *Geology* **24**, 807–810 (1996).
5. Levin, L. A. in *Oceanography and Marine Biology Vol. 43* (eds Gibson, R. N., Atkinson, R. J. A. & Gordon, J. D. M) 1–46 (CRC, 2005).
6. Sibuet, M. & Olu, K. Biogeography, biodiversity and fluid dependence of deep-sea cold-seep communities at active and passive margins. *Deep Sea Res. II* **45**, 517–567 (1998).
7. Aguilar Pérez, M. I., Zapata-Ramírez, P. A. & Micallef, A. A review of cold seeps in the Western Atlantic, focusing on Colombia and the Caribbean. *Front. Mar. Sci.* **11**, 1430377 (2024).
8. Cordes, E. E. et al. The influence of geological, geochemical, and biogenic habitat heterogeneity on seep biodiversity. *Mar. Ecol.* **31**, 51–65 (2010).
9. Lonsdale, P. Clustering of suspension-feeding macrobenthos near abyssal hydrothermal vents at oceanic spreading centers. *Deep Sea Res.* **24**, 857–863 (1977).
10. Oliver, P. G. & Chen, C. Revision of the generic placement of two hadal bivalves (Bivalvia: Thysiridae) from the Japan Trench, with the introduction of a new genus *Tartarothyas*. *J. Conchol.* **45**, 35–50 (2024).
11. Hand, K. P. et al. Discovery of novel structures at 10.7 km depth in the Mariana Trench may reveal chemolithosutrophic microbial communities. *Deep Sea Res. I* **160**, 103238 (2020).
12. Davaille, A. & Lees, J. M. Thermal modeling of subducted plates: tear and hot spot at the Kamchatka corner. *Geophys. Res. Lett.* **27**, 3663–3666 (2000).
13. Jamieson, A. J. & Stewart, H. A. Hadal zones of the Northwest Pacific Ocean. *Prog. Oceanogr.* **190**, 102477 (2021).
14. Brandt, A., Brix, S., Riehl, T. & Malyutina, M. Biodiversity and biogeography of the abyssal and hadal Kuril–Kamchatka trench and adjacent NW Pacific deep-sea regions. *Prog. Oceanogr.* **181**, 102232 (2020).
15. Kamenev, G. M. et al. Macrofauna and nematode abundance in the abyssal and hadal zones of interconnected deep-sea ecosystems in the Kuril Basin (Sea of Okhotsk) and the Kuril–Kamchatka Trench (Pacific Ocean). *Front. Mar. Sci.* **9**, 812464 (2022).
16. Mironov, A. N., Krylova, E. M. & Drozdov, A. L. Specific taxonomic and trophic structure of hadal benthic communities. In *Abstracts of the 9th Deep-Sea Biology Symposium* (National Univ. of Ireland, 2000).
17. Shunakov, V. P. *Biology of Far-Eastern Seas of Russia Vol. 1* (TINRO-Center, 2001).
18. Klaeschen, D., Belykh, I., Gnibidenko, H., Patrikeyev, S. & von Huene, R. Structure of the Kuril Trench from seismic reflection records. *J. Geophys. Res. Solid Earth* **99**, 24173–24188 (1994).
19. Suess, E. et al. Fluid venting in the eastern Aleutian subduction zone. *J. Geophys. Res. Solid Earth* **103**, 2597–2614 (1998).
20. Sasaki, T., Okutani, T. & Fujikura, K. Molluscs from hydrothermal vents and cold seeps in Japan: a review of taxa recorded in twenty recent years (1984–2004). *Venus* **64**, 87–133 (2005).
21. Okutani, T., Fujikura, K., Watanabe, H. & Ohara, Y. *Calyptogena (Abyssogena) mariana*: discovery of a new vesicomyid clam from the Mariana Trench. *Venus* **71**, 39–47 (2013).
22. Okumura, T. et al. Brucite chimney formation and carbonate alteration at the Shinkai SeepField, a serpentinite-hosted vent system in the southern Mariana forearc. *Geochem. Geophys. Geosyst.* **17**, 3775–3796 (2016).
23. Jeffrey, A. W. A., Pflaum, R. C., McDonald, T. J., Brooks, J. M. & Kvenvolden, K. A. in *Initial Reports of the Deep Sea Drilling Project Leg Vol. 84* (ed. Orlofsky, S.) 719–726 (US Government Printing Office, 1985).
24. Kvenvolden, K. A. A review of the geochemistry of methane in natural gas hydrate. *Org. Geochem.* **23**, 997–1008 (1995).
25. Schoell, M. Multiple origins of methane in the Earth. *Chem. Geol.* **71**, 1–10 (1988).
26. Mayumi, D. et al. Hydrogenotrophic methanogens overwrite isotope signals of subsurface methane. *Science* **386**, 1372–1376 (2024).
27. Bueno de Mesquita, J., Wu, D. & Tringe, S. G. Methyl-based methanogenesis: an ecological and genomic review. *Microbiol. Mol. Biol. Rev.* **87**, e0002422 (2023).
28. Milkov, A. V. & Etiope, G. Revised genetic diagrams for natural gases based on a global dataset of >20,000 samples. *Org. Geochem.* **125**, 109–120 (2018).
29. Joye, S. B., Bowles, M. W., Samarkin, V. A., Hunter, K. S. & Niemann, H. Biogeochemical signatures and microbial activity of different cold-seep habitats along the Gulf of Mexico deep slope. *Deep Sea Res. II* **57**, 1990–2001 (2010).
30. Liu, W. et al. Pore-water dissolved inorganic carbon sources and cycling in the shallow sediments of the Haimea cold seeps, South China Sea. *J. Asian Earth Sci.* **201**, 104495 (2020).
31. Reitz, A. et al. Sources of fluids and gases expelled at cold seeps offshore Georgia, eastern Black Sea. *Geochim. Cosmochim. Acta* **75**, 3250–3268 (2011).
32. Suess, E. et al. Calcium carbonate hexahydrate from organic-rich sediments of the Antarctic Shelf: precursors of glendonites. *Science* **216**, 1128–1131 (1982).
33. Rathburn, A. E. et al. Geological and biological heterogeneity of the Aleutian Margin (1965–4822 m). *Prog. Oceanogr.* **80**, 22–50 (2009).
34. Watson, S. J. et al. Focused fluid seepage related to variations in accretionary wedge structure, Hikurangi Margin, New Zealand. *Geology* **48**, 56–61 (2019).
35. Riedel, M. et al. Distributed natural gas venting offshore along the Cascadia margin. *Nat. Commun.* **9**, 3264 (2018).
36. Floodgate, G. & Judd, A. G. The origins of shallow gas. *Cont. Shelf Res.* **12**, 1145–1156 (1992).
37. Parkes, R. J., Cragg, B. A., Fry, J. C., Herbert, R. A. & Wimpenny, J. T. Bacterial biomass and activity in deep sediment layers from the Peru margin. *Proc. R. Soc. Lond. A* **391**, 139–153 (1990).
38. Danovaro, R., Della Croce, N., Dell'Anno, A. & Pusceddu, A. A depocenter of organic matter at 7800 m depth in the SE Pacific Ocean. *Deep Sea Res. I* **50**, 1411–1420 (2003).
39. Glud, R. N. et al. High rates of microbial carbon turnover in sediments in the deepest oceanic trench on Earth. *Nat. Geosci.* **6**, 284–288 (2013).
40. Glud, R. N. et al. Hadal trenches are dynamic hotspots for early diagenesis in the deep sea. *Commun. Earth Environ.* **2**, 21 (2021).

41. Itou, M. A large flux of particulate matter in the deep Japan Trench observed just after the 1994 Sanriku-Oki earthquake. *Deep Sea Res. I* **47**, 1987–1998 (2000).
42. Hyndman, R. D. & Davis, E. E. A mechanism for the formation of methane hydrate and seafloor bottom-simulating reflectors by vertical fluid expulsion. *J. Geophys. Res.* **97**, 7025–7041 (1992).
43. Stockton, W. L. & DeLaca, T. E. Food falls in the deep sea: occurrence, quality, and significance. *Deep Sea Res. A* **29**, 157–169 (1982).
44. Åström, E. K. L., Bluhm, B. A. & Rasmussen, T. L. Chemosynthetic and photosynthetic trophic support from cold seeps in Arctic benthic communities. *Front. Mar. Sci.* **9**, 910558 (2022).
45. Bradley, J. A. et al. Widespread energy limitation to life in global subseafloor sediments. *Sci. Adv.* **6**, eaba0697 (2020).
46. Parkes, R. J., Cragg, B. A. & Wellsbury, P. Recent studies on bacterial populations and processes in subseafloor sediments: a review. *Hydrogeol. J.* **8**, 11–28 (2000).
47. Harrison, W. E. & Curiale, J. A. in *Initial Reports of the Deep Sea Drilling Project Vol. 67* (eds Aubouin, J. et al.) 591–594 (US Government Printing Office, 1982).
48. Kvenvolden, K. A. & Kastner, M. Gas hydrates of the Peruvian outer continental margin. *Proc. Ocean Drill. Prog. Sci. Results* **112**, 517–526 (1990).
49. Kelemen, P. B. & Manning, C. E. Reevaluating carbon fluxes in subduction zones, what goes down, mostly comes up. *Proc. Natl Acad. Sci. USA* **112**, E3997–E4006 (2015).
50. Plank, T. & Manning, C. E. Subducting carbon. *Nature* **574**, 343–352 (2019).

Publisher's note Springer Nature remains neutral with regard to jurisdictional claims in published maps and institutional affiliations.



Open Access This article is licensed under a Creative Commons Attribution-NonCommercial-NoDerivatives 4.0 International License, which permits any non-commercial use, sharing, distribution and reproduction in any medium or format, as long as you give appropriate credit to the original author(s) and the source, provide a link to the Creative Commons licence, and indicate if you modified the licensed material. You do not have permission under this licence to share adapted material derived from this article or parts of it. The images or other third party material in this article are included in the article's Creative Commons licence, unless indicated otherwise in a credit line to the material. If material is not included in the article's Creative Commons licence and your intended use is not permitted by statutory regulation or exceeds the permitted use, you will need to obtain permission directly from the copyright holder. To view a copy of this licence, visit <http://creativecommons.org/licenses/by-nc-nd/4.0/>.

© The Author(s) 2025

Article

Methods

The investigation was carried out during TS42 cruise between 7 July and 18 August 2024 by RV *Tan Suo Yi Hao* with the full-ocean-depth human-occupied vehicle *Fendouzhe*, which was fitted with hydraulically powered manipulators on two swing arms. Under the guidance of operators in the human-occupied vehicle, the arms efficiently acquired the samples and stored them safely in a biological box and a geological box of the vehicle.

Processing of benthic fauna and sea floor video footage

Upon retrieval of the submersible, all collected specimens were promptly transferred from the biological collection box and slurp sampler to the shipboard laboratory. The specimens were then sorted into main taxonomic groups of different levels using visual inspection or under stereomicroscopes. Each organism was counted and preserved in pre-cooled, non-denatured 95% ethanol or in a 4% buffered formaldehyde solution depending on the taxon. Following initial preservation, certain taxonomic groups were further transferred to 70% ethanol for long-term storage.

Visual assessment of species identification, density and spatial structure of the macro-epifauna and mega-epifauna of the seep communities was carried out on the basis of the analysis of video footage recorded by two high-definition cameras mounted on the human-occupied vehicle. For each dive, between three and ten representative screenshots showing the densest cold-seep communities were selected from the video footage. The area of each image was estimated using the submersible's laser scale, which projects two parallel laser points 10 cm apart onto the sea floor. This provided a reliable spatial reference for calculating the area of the sea floor captured in each image. A standardized quadrat (for example, 50 × 50 cm) was drawn near the laser dots by using this laser scale as a reference in the image. The calculated area was then converted into square metres for standardized density calculations. Animals visible in each quadrat were manually counted, and faunal density was expressed as the number of individuals per square metre. For each dive, density values from the selected images were used to calculate the mean faunal density, and the standard deviation was computed to quantify the variability among replicate images.

Phylogenetic analyses of the *cox1*/gene sequences

Up to 0.5 cm³ of fauna tissue was cut into tiny pieces and subjected to DNA extraction using the PowerSoil DNA Isolation kit (MoBio Laboratories). The extracted DNA was quantified using a Qubit dsDNA HS Assay Kit with Qubit 2.0 fluorometer (Invitrogen). A metagenomic library was constructed using the VAHTS Universal DNA Library Prep Kit for Illumina v.4 and sequenced on the NovaSeq X Plus platform (Illumina) to generate 2 × 150 bp pair-ended reads. Raw sequencing reads were qualified using Fastp v.0.23.2 and assembled into contigs using MEGAHIT v.1.2.9. The *cox1* gene encoding cytochrome c oxidase subunit I of the fauna was retrieved from metagenomic contigs. The retrieved *cox1* was searched against the National Center for Biotechnology Information GenBank database for preliminary taxonomy identification.

Gas and pore-water sampling

During each dive, 6–12 sediment pushcores were collected using the manipulators of the submersible. Upon recovery, these pushcores were immediately transported to the ship's cold room, which is kept at around 4 °C, to facilitate subsequent processing. Among them, one or two pushcores were allocated for gas concentration analysis onboard, with only subsamples exhibiting high methane concentrations being prepared for further carbon and deuterium isotope analysis. In addition, one or two pushcores were used to extract pore water samples for geochemical analysis.

Pore-water sampling was conducted using Rhizon samplers (as described in ref. 51). These samplers were inserted into the cores at 2-cm intervals and connected to 50-ml evacuated disposable syringes

fitted with three-way Luer-lock stopcocks. The first approximately 1 ml of extracted pore water was discarded to remove any contaminants. Subsequently, around 15 ml of pore water was collected within a 2-h time frame. One portion of the pore water was preserved with a 20% zinc acetate solution for subsequent hydrogen sulfide analysis. The remaining pore water samples were transferred to 15-ml centrifuge tubes and frozen for subsequent ion analysis.

For the analysis of gas composition and isotopes, sediment samples were collected using a 2.5-ml cutoff plastic syringe, which was inserted through pre-drilled holes in the pushcore tube at depth intervals of 4 cm. A 2.5-ml sediment sample was then transferred to a 20-ml gas-tight glass vial, which was filled with 2 M NaOH solution and sealed with a crimp cap containing butyl rubber stoppers. The vials were vigorously shaken and stored in an upside-down position at 4 °C until analysis, which was conducted onboard in a single day. Before analysis, the vials were shaken again, and 2 ml of the NaOH solution was replaced with helium gas to create a headspace. The headspace gas from the push core was also directly extracted using a 20-ml syringe equipped with a three-way stopcock and was immediately transferred to a 12-ml vacuum Labco vial for further analysis.

Gas concentration and isotope

The concentration of dissolved gases was determined using a gas chromatograph (Trace GC1310; Thermo Scientific) installed onboard the research vessel. Headspace volumes ranging from 100 to 500 µl were sampled and injected into a gas chromatograph equipped with a flame ionization detector. The analytical precision achieved in these measurements is consistently lower than 5%.

The $\delta^{13}\text{C}$ and δD isotopic compositions of methane were analysed using a gas chromatography-isotope ratio mass spectrometer system, which consisted of a Trace GC1310 connected to a Delta V Advantage Isotope Ratio MS (Thermo Scientific). The analysis was conducted at the Institute of Deep-Sea Science and Engineering (IDSSE), Chinese Academy of Sciences.

Methane was selectively separated from the gas matrix using a gas chromatography column (27 m × 0.3 mm × 20.00 µm; PoraPLOT Q). The separated methane was then combusted in a combustion oven at a temperature of 1,000 °C, which was interfaced with the isotope ratio mass spectrometer (IRMS) for subsequent analysis. The resulting CO₂ was directly introduced into the IRMS for measurement.

The precision of the repeated analyses, expressed as the standard deviation (1σ), was $\pm 0.5\%$ for $\delta^{13}\text{C}$ and $\pm 2\%$ for δD. The isotopic compositions of individual carbon compounds were reported as δ-values (‰) relative to the international standards Vienna PeeDee Belemnite (VPDB) for $\delta^{13}\text{C}$ and Vienna Standard Mean Ocean Water (VSMOW) for δD.

Pore-water geochemistry

Hydrogen sulfide concentrations were determined colorimetrically using the methylene blue method (with a limit of detection of approximately 0.5 µM). The concentration of SO₄²⁻ in pore water was quantified by ion chromatography using a Dionex ICS-900 system, which was equipped with an AS50 AutoSampler. To ensure that the SO₄²⁻ concentrations fell in the optimal analytical range for the ion chromatograph, the anion samples were diluted 70-fold with Milli-Q water. The analytical precision for the determination of SO₄²⁻ was $\pm 3.0\%$. NH₄⁺ concentrations were measured using a fluorescence spectrometer (LS55, PE) following the procedure reported in ref. 52, with a relative deviation of 0.5%. DIC concentrations and $\delta^{13}\text{C}$ -DIC values were analysed using a Gas Bench II IRMS at IDSSE. The samples were pretreated with an acid solution on the Gas Bench II; the resulting carbon dioxide, carried by helium, was separated by a constant-temperature chromatographic column and subsequently analysed for isotope abundance using a MAT253 gas stable IRMS. The analytical precision for DIC was $\pm 0.15\%$ and that for $\delta^{13}\text{C}$ -DIC was $\pm 0.5\%$. Dissolved organic carbon concentrations were measured by a high-temperature catalytic oxidation method

using a Multi N/C 3100 (CLD) analyser at IDSSE. Samples were thawed at room temperature and acidified to pH 2 with 2 mol l⁻¹ hydrochloric acid before injection. Salinity was measured in the laboratory using a handheld digital salinity meter (ATAGO PAL-SALT) after the samples were thawed to room temperature.

Methane phase modelling

The phase boundaries and methane hydrate solubility in the methane hydrate–sea water system were calculated using thermodynamic models^{53,54}. The chemical potential of the hydrate phase was determined through the application of the Van der Waals–Platteeuw hydrate model, in conjunction with angle-dependent ab initio intermolecular potentials, as previously described in ref. 55. The Gibbs–Thomson equation, incorporating appropriately parameterized hydrate–water interface values, was used to account for the capillary effects of porous sediments on the hydrate–liquid–vapour equilibrium and the hydrate–liquid equilibrium. The influence of surface textures and mineral components was neglected in this analysis.

The activity coefficients for water and methane in the methane–sea water system were calculated using the Pitzer model. By applying the Poynting correction to the fugacity of methane dissolved in aqueous solution at the hydrate–liquid equilibrium, where methane gas is absent, the extended model for three-phase equilibrium was adapted to predict the solubility of methane in aqueous solution at the hydrate–liquid equilibrium.

Reporting summary

Further information on research design is available in the Nature Portfolio Reporting Summary linked to this article.

Data availability

The *cox*/gene sequences of six chemosynthetic invertebrates have been deposited in the GenBase database under accession numbers C_AA106802 to C_AA106807 and are publicly accessible at <https://ngdc.cncb.ac.cn/genbase>.

51. Seeberg-Elverfeldt, J., Schluter, M., Feseker, T. & Kolling, M. Rhizon sampling of porewaters near the sediment–water interface of aquatic systems. *Limnol. Oceanogr. Methods* **3**, 361–371 (2005).
52. Holmes, R. M., Aminot, A., Kerouel, R., Hooker, B. A. & Peterson, B. J. A simple and precise method for measuring ammonium in marine and freshwater ecosystems. *Can. J. Fish. Aquat. Sci.* **56**, 1801–1808 (1999).
53. Duan, Z. & Sun, R. A model to predict phase equilibrium of CH₄ and CO₂ clathrate hydrate in aqueous electrolyte solutions. *Am. Mineral.* **91**, 1346–1354 (2006).
54. Sun, R. & Duan, Z. Prediction of CH₄ and CO₂ hydrate phase equilibrium and cage occupancy from ab initio intermolecular potentials. *Geochim. Cosmochim. Acta* **69**, 4411–4424 (2005).
55. Sun, R. & Duan, Z. An accurate model to predict the thermodynamic stability of methane hydrate and methane solubility in marine environments. *Chem. Geol.* **244**, 248–262 (2007).

Acknowledgements We thank the crews, pilots and scientists aboard RV *Tan Suo Yi Hao* with full-ocean-depth human-occupied vehicle *Fendouzhe*. X.P. and M.D. are supported by the National Key R&D Program of China (grant no. 2022YFC2805400), the Program for Fostering International Mega-Science of the Chinese Academy of Sciences (grant no. 183446KY SB20210002), and the Hainan Provincial Outstanding Talent Team Program ‘Research, Operation, and Application Team for Specialized Large-Scale Deep-Sea Submersible Equipment’. V.V.M. is supported by the Ministry of Science and Higher Education of the Russian Federation for NSCMB FEB RAS (project reg. nos. 124021900009-6 and 124021900011-9). A.G. is supported by the Russian Science Foundation (grant no. 24-17-00321). This work was under the scheme of the Global Trench Exploration and Dive Programme (Global TRENd).

Author contributions X.P., M.D., A.G. and V.V.M. conceived the research. M.D., Shuangquan Liu, Shuting Liu, X.P., P.Z. and T.X. performed the geochemical measurements. A.G., G.M.K., A.S. M., I.L.A., I.Yu.D., M.V.M., A.A.S., V.A.S., A.V.A., Z.G. and V.M. contributed to fauna data analysis. R.W. performed methane phase modelling. X.P., M.D., Shuangquan Liu, R.N.G., D.P., T.X. and Y.Q. contributed to the geochemical data interpretation. Z.G., A.R., A.G., A.V.A., X.P., M.D., X.S. and V.V.M. contributed to the fauna data interpretation. M.D., X.P., Shuangquan Liu, P.Z., A.G., G.M.K., S.C., Hao Liu, J.G., Z.G., Y.H., H.X., Hanyu Zhang, X.L., S.D., A.S.M., M.V.M., A.A.S., V.A.S., Haibin Zhang, W.X., Helu Liu, W.Z., X.H. and V.V.M. conducted the cruise and collected samples. All co-authors participated in the discussion. X.P., M.D. and V.V.M. wrote the manuscript with input from all co-authors.

Competing interests The authors declare no competing interests.

Additional information

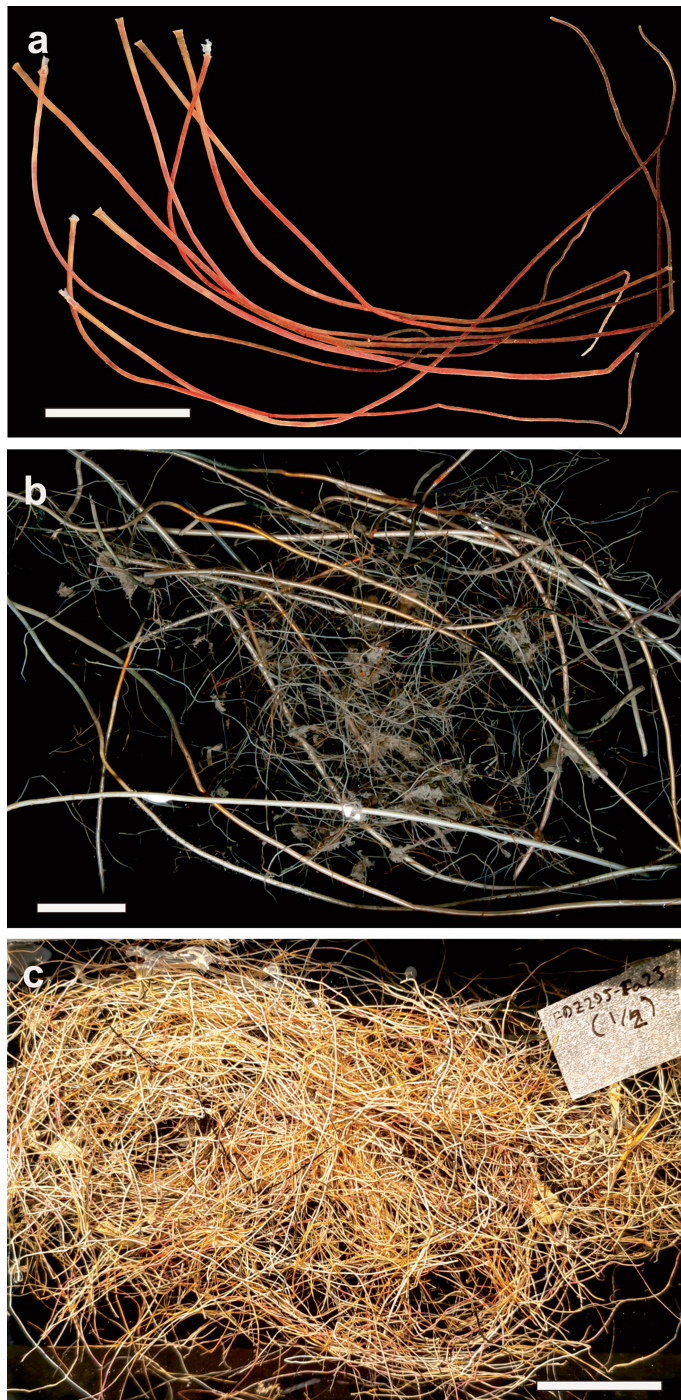
Supplementary information The online version contains supplementary material available at <https://doi.org/10.1038/s41586-025-09317-z>.

Correspondence and requests for materials should be addressed to Mengran Du or Vladimir V. Mordukhovich.

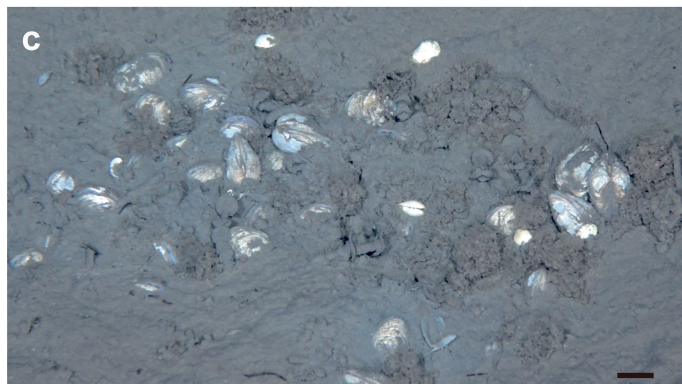
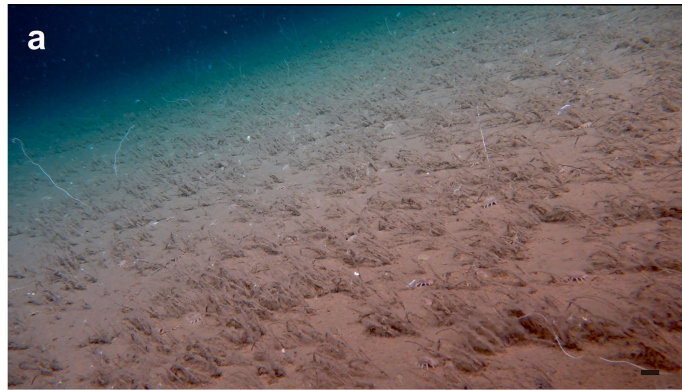
Peer review information *Nature* thanks Lisa Levin, April Stabbins and Andreas Teske for their contribution to the peer review of this work. Peer reviewer reports are available.

Reprints and permissions information is available at <http://www.nature.com/reprints>.

Article



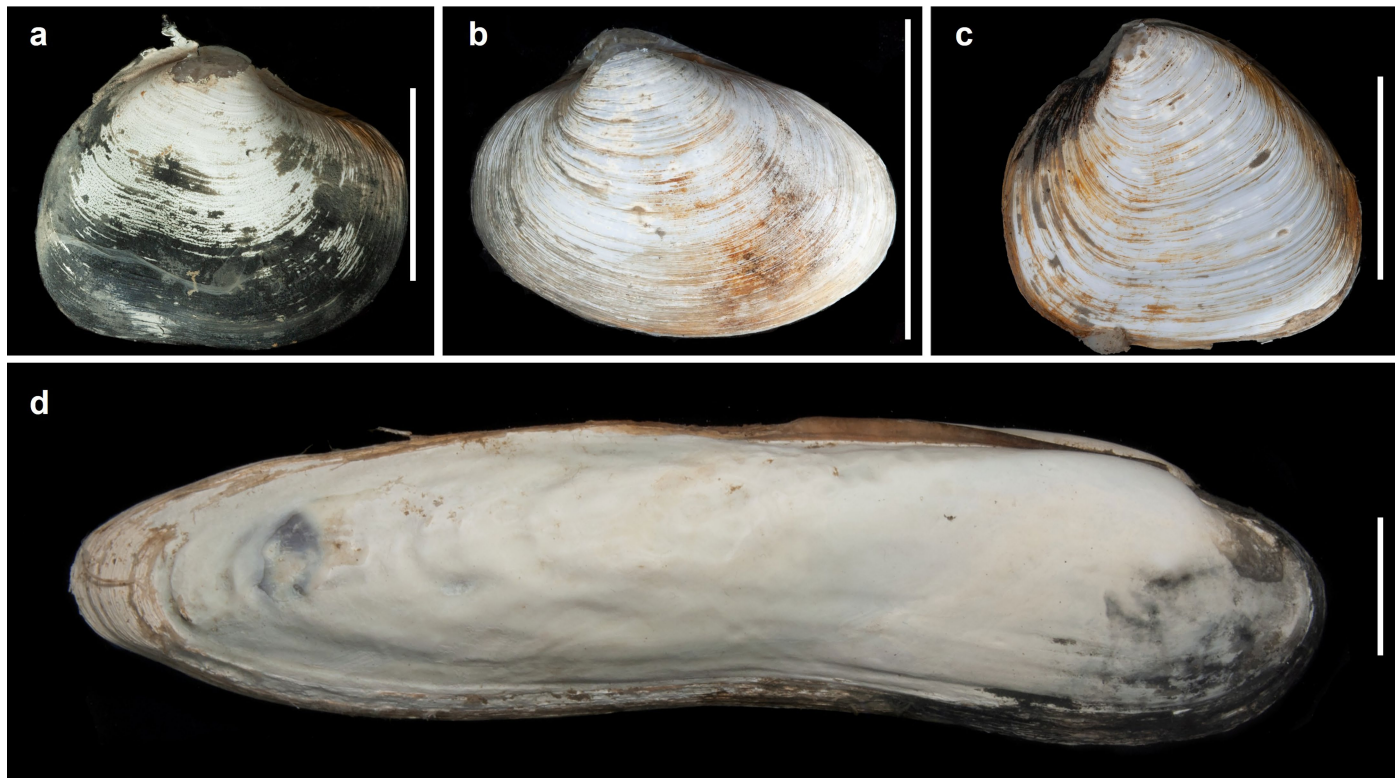
Extended Data Fig. 1 | Some samples of Siboglinidae collected during cruise. **a**, FDZ 271, short tubeworms cf. *Spirobranchia* (from the Deepest seep field). **b**, FDZ 294, mix of ultra slender & long wide tubeworms (from Blue Marsh, Icy River). **c**, FDZ 295, beard of ultra slender tubeworms (from Blue Marsh, Icy River). Scale bars=20 mm.



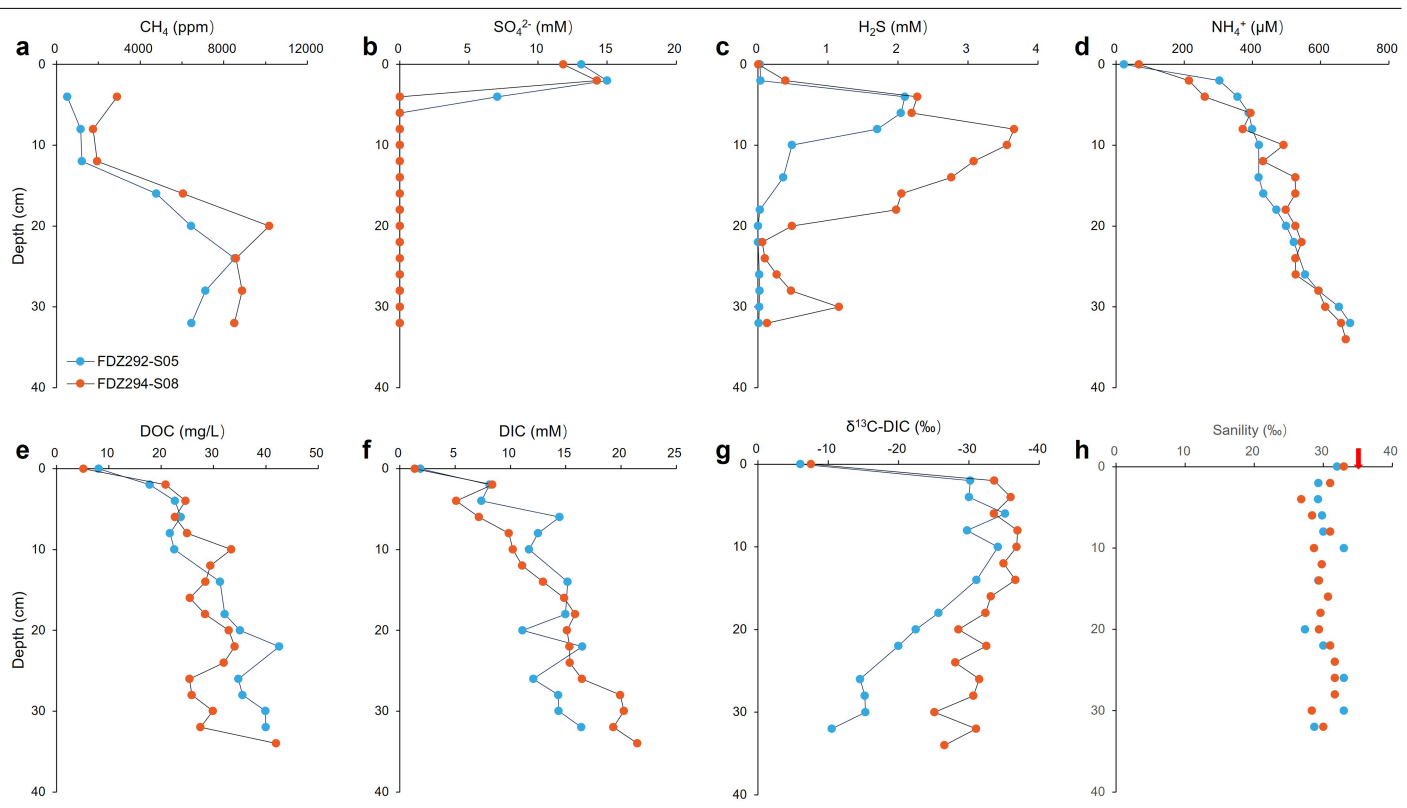
Extended Data Fig. 2 | Representative fauna at three hadal cold seeps.

a, Dead Valley. **b**, Clam Valley. **c**, Turtle Egg. Scale bars=20 mm.

Article



Extended Data Fig. 3 | Representative samples of Bivalvia recovered from seeps. **a**, FDZ 286, *Tartarothyasira* cf. *hadalis*. **b**, FDZ 296, *Isorropodon fossajaponicum*. **c**, FDZ 298, *Axinus* sp. **d**, FDZ 297, *Abyssogenaphaseoliformis*. Scale bars=20 mm.

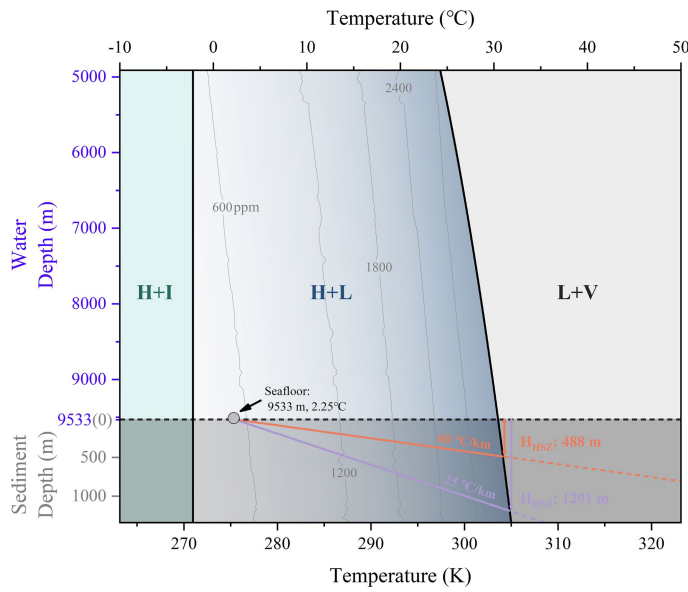


Extended Data Fig. 4 | Vertical profiles of porewater geochemistry in two sediment pushcores (FDZ292-S05 and FDZ294-S08). **a**, CH₄. **b**, SO₄²⁻. **c**, H₂S. **d**, NH₄⁺. **e**, DOC. **f**, DIC. **g**, δ¹³C-DIC. **h**, Salinity.

Article



Extended Data Fig. 5 | Representative ikaite samples recovered from cold seeps. a, Ikaite specimens. **b,** Photomicrograph of ikaite. Scale bar=1 cm in a and 2 mm in b.



Extended Data Fig. 6 | A phase diagram illustrating hydrate stability conditions in the sediments of the investigated hadal zone. The horizontal black dashed line denotes the 9,533-meter water depth, corresponding to 98.0 MPa of hydrostatic pressure (assuming an average water density of 1.045 g/cm³), above which lies the unconsolidated sub-seafloor sediments. The gray circle denotes the seafloor temperature-pressure conditions at 9,533 meters, with a temperature of 2.25 °C and a pressure of 98.0 MPa. The purple and red lines represent the minimum and maximum geothermal gradients (ranging from 25 to 60 °C/km) within the unconsolidated sediments, respectively. The point of intersection between these geothermal gradients and HLV delineates the vertical limits of the hydrate stability zone (HSZ) within the sediment.

Article



Extended Data Fig. 7 | A coexistence example of frenulate siboglinids with *Elpidia hansenii*. FDZ 271, at 9532 m at The Deepest. Scale bar=3 cm.

Extended Data Table 1 | Typical chemosynthetic invertebrates and their close relatives based on coxI gene sequences

Sample ID	Description	Subject sequence	Subject sequence source	Identity (%)	Alignment length
FDZ 271 ^a	Slender tubeworms	FJ480373	<i>Spirobranchia tripeira</i> isolate AT622-G5	92.93	848
FDZ 294 ^b	Ultra slender tubeworms	FJ480373	<i>Spirobranchia tripeira</i> isolate AT622-G16	92.59	850
FDZ 286 ^c	<i>Tartarothyasira</i> cf. <i>hadalis</i>	JLC187042	<i>Axinulus hadalis</i> coxI	98.36	487
FDZ 296 ^d	<i>Isorropodon fossajaponicum</i>	AP014550	<i>Isorropodon fossajaponicum</i>	99.93	1524
FDZ 298 ^e	<i>Axinus</i> sp. (Morphology identification)	PP334094	<i>Thyasira obsoleta</i> isolate M5	83.05	655
FDZ 297 ^f	<i>Abyssogena phaseoliformis</i>	AP014557	<i>Abyssogena phaseoliformis</i> coxI	100	1653

* The data have been deposited in the GenBase in National Genomics Data Center, Beijing Institute of Genomics, Chinese Academy of Sciences, under accession number C_AA106802.1 to C_AA106807.1, which is publicly accessible at <https://hgdc.cncb.ac.cn/genbase>.

Article

Extended Data Table 2 | Gas compositions and isotopic compositions of gases from cold seep sediment cores

No. of sample	CH ₄	C ₂ H ₆	CO ₂	H ₂	CO	¹³ C-CH ₄	¹³ C-CO ₂	¹³ D-CH ₄
	Ppm					‰		
FDZ284-S03 Gas-20cm	7613.63	bd	67.88	bd	bd	-90.43	bd	-158.93
FDZ284-S03 Gas-24cm	6828.00	bd	66.70	bd	bd	-90.90	bd	-175.55
FDZ284-S03 Gas-28cm	8863.23	bd	91.30	bd	bd	-88.68	bd	-171.63
FDZ284-S03 Gas-32cm	7922.78	bd	83.98	bd	bd	-89.16	bd	-187.33
FDZ284-S03 Gas-36cm	7447.00	bd	87.14	bd	bd	-88.62	bd	-188.75
FDZ286-S08 Gas-8cm	10000.74	bd	47.03	bd	bd	-90.84	bd	-176.34
FDZ286-S08 Gas-12cm	13892.28	bd	66.35	bd	bd	-90.16	bd	-158.08
FDZ286-S08 Gas-16cm	9819.99	bd	66.52	bd	bd	-84.23	bd	-175.02
FDZ286-S08 Gas-20cm	14097.19	bd	62.62	bd	bd	-82.66	bd	-163.95
FDZ286-S08 Gas-24cm	14717.00	bd	70.21	bd	bd	-81.46	bd	-166.79
FDZ292-S05 Gas-20cm	6956.92	bd	49.05	bd	bd	-88.76	bd	-161.34
FDZ292-S05 Gas-24cm	8872.02	bd	58.87	bd	bd	-84.96	bd	-168.18
FDZ292-S05 Gas-28cm	9001.59	bd	39.93	bd	bd	-82.88	bd	-172.30
FDZ292-S05 Gas-32cm	8225.00	bd	130.40	bd	bd	-81.54	bd	-170.20
FDZ292-S06 Gas-16cm	5569.61	bd	78.19	bd	bd	-95.74	bd	-158.42
FDZ292-S06 Gas-20cm	7227.83	bd	49.27	bd	bd	-93.73	bd	-167.22
FDZ292-S06 Gas-24cm	6096.20	bd	59.79	bd	bd	-87.79	bd	-173.66
FDZ292-S06 Gas-28cm	9682.76	bd	59.42	bd	bd	-84.59	bd	-161.49
FDZ292-S06 Gas-32cm	10428.51	bd	23.73	bd	bd	-83.92	bd	-166.26
FDZ292-S06 Gas-36cm	6811.00	bd	108.80	bd	bd	-83.53	bd	-181.22
FDZ294-S08 Gas-16cm	6688.36	bd	54.04	bd	bd	-89.96	bd	-165.89
FDZ294-S08 Gas-20cm	9885.48	bd	140.60	bd	bd	-82.14	bd	-156.94
FDZ294-S08 Gas-24cm	7969.40	bd	18.18	bd	bd	-86.81	bd	-167.51
FDZ294-S08 Gas-32cm	9954.00	bd	98.55	bd	bd	-85.66	bd	-168.95
FDZ295-S01 Gas-12cm	12249.50	bd	17.04	bd	bd	-84.25	bd	-164.76
FDZ295-S01 Gas-16cm	12525.71	bd	10.31	bd	bd	-83.14	bd	-167.63
FDZ295-S01 Gas-20cm	13716.04	bd	25.54	bd	bd	-85.23	bd	-167.19
FDZ295-S01 Gas-28cm	11349.00	bd	323.00	bd	bd	-83.21	bd	-173.48
FDZ295-S04 Gas-12cm	13286.67	bd	12.77	bd	bd	-81.38	bd	-159.08
FDZ295-S04 Gas-16cm	13098.98	bd	11.62	bd	bd	-78.11	bd	-169.66
FDZ295-S04 Gas-24cm	16377.00	bd	109.10	bd	bd	-78.22	bd	-161.58
FDZ274 S04-26 cm	5398.2	bd	260.81	bd	bd	-82.57	bd	-170.20
FDZ286 PC Head gas	87554	bd	649.84	7.92	18.78	-82.29	-11.71	-172.59
FDZ286-1 PC head gas	110357	bd	bd	bd	bd	-85.67	-11.24	-164.92
FDZ292-PC05 head gas-2	118882	bd	568.67	8.20	19.15	-85.00	-17.03	-153.99
FDZ292-PC05 head gas-4	133159	bd	bd	bd	bd	-84.84	-15.25	-152.90
FDZ292-PC06 head gas-1	98290	bd	567.84	7.22	16.40	-86.30	-16.05	-160.59
FDZ297-PC head gas-1	27681	3.00	547.57	5.27	bd	-89.41	-17.83	-142.21

* bd: below detection.

Extended Data Table 3 | Carbon and oxygen isotope of ikaite

No. of sample	$\delta^{13}\text{C}_{\text{V-PDB}} \text{\textperthousand}$	$\delta^{18}\text{O}_{\text{V-PDB}} \text{\textperthousand}$
FDZ271-S05-14cm	-17.58	-0.19
FDZ271-S05-16cm	-17.29	0.24
FDZ271-S05-18cm	-17.98	-0.10
FDZ271-S05-20cm	-19.70	1.72
FDZ284-S03-12cm	-22.46	-3.13
FDZ285-ikaite-01	-24.63	1.07
FDZ285-ikaite-02	-23.11	-2.79
FDZ296-ikaite-02	-26.56	0.36
FDZ296-ikaite-05	-26.30	0.53
FDZ296-ikaite-08	-26.89	1.73
FDZ296-ikaite-11	-25.89	0.53
FDZ296-ikaite-01	-25.71	-2.86
FDZ296-ikaite-09	-25.21	-3.59

Reporting Summary

Nature Portfolio wishes to improve the reproducibility of the work that we publish. This form provides structure for consistency and transparency in reporting. For further information on Nature Portfolio policies, see our [Editorial Policies](#) and the [Editorial Policy Checklist](#).

Statistics

For all statistical analyses, confirm that the following items are present in the figure legend, table legend, main text, or Methods section.

n/a Confirmed

- The exact sample size (n) for each experimental group/condition, given as a discrete number and unit of measurement
- A statement on whether measurements were taken from distinct samples or whether the same sample was measured repeatedly
- The statistical test(s) used AND whether they are one- or two-sided
Only common tests should be described solely by name; describe more complex techniques in the Methods section.
- A description of all covariates tested
- A description of any assumptions or corrections, such as tests of normality and adjustment for multiple comparisons
- A full description of the statistical parameters including central tendency (e.g. means) or other basic estimates (e.g. regression coefficient) AND variation (e.g. standard deviation) or associated estimates of uncertainty (e.g. confidence intervals)
- For null hypothesis testing, the test statistic (e.g. F , t , r) with confidence intervals, effect sizes, degrees of freedom and P value noted
Give P values as exact values whenever suitable.
- For Bayesian analysis, information on the choice of priors and Markov chain Monte Carlo settings
- For hierarchical and complex designs, identification of the appropriate level for tests and full reporting of outcomes
- Estimates of effect sizes (e.g. Cohen's d , Pearson's r), indicating how they were calculated

Our web collection on [statistics for biologists](#) contains articles on many of the points above.

Software and code

Policy information about [availability of computer code](#)

Data collection

N/A

Data analysis

Global Mapper 14

For manuscripts utilizing custom algorithms or software that are central to the research but not yet described in published literature, software must be made available to editors and reviewers. We strongly encourage code deposition in a community repository (e.g. GitHub). See the Nature Portfolio [guidelines for submitting code & software](#) for further information.

Data

Policy information about [availability of data](#)

All manuscripts must include a [data availability statement](#). This statement should provide the following information, where applicable:

- Accession codes, unique identifiers, or web links for publicly available datasets
- A description of any restrictions on data availability
- For clinical datasets or third party data, please ensure that the statement adheres to our [policy](#)

The coxl gene sequences of six chemosynthetic invertebrates have been deposited in the GenBase database under accession number C_AA106802 to C_AA106807 and are publicly accessible at <http://ngdc.cncb.ac.cn/genbase>.

Research involving human participants, their data, or biological material

Policy information about studies with [human participants or human data](#). See also policy information about [sex, gender \(identity/presentation\), and sexual orientation](#) and [race, ethnicity and racism](#).

Reporting on sex and gender	<input type="text" value="N/A"/>
Reporting on race, ethnicity, or other socially relevant groupings	<input type="text" value="N/A"/>
Population characteristics	<input type="text" value="N/A"/>
Recruitment	<input type="text" value="N/A"/>
Ethics oversight	<input type="text" value="N/A"/>

Note that full information on the approval of the study protocol must also be provided in the manuscript.

Field-specific reporting

Please select the one below that is the best fit for your research. If you are not sure, read the appropriate sections before making your selection.

Life sciences Behavioural & social sciences Ecological, evolutionary & environmental sciences

For a reference copy of the document with all sections, see nature.com/documents/nr-reporting-summary-flat.pdf

Ecological, evolutionary & environmental sciences study design

All studies must disclose on these points even when the disclosure is negative.

Study description	We used human occupied vehicle to discover the deepest chemosynthetic communities in hadal trench
Research sample	All chemosynthetic communities observed during dives were described and sampled
Sampling strategy	We used the manipulators and slurp sampler of the HOV to recover all tubeworm and bivalve samples
Data collection	Assessment of species, abundance and spatial structure based on video and microscope. Geochemistry data of sediment and porewater were collected onboard and on-land laboratory. Cruise participants collected onboard data and laboratory data.
Timing and spatial scale	Onboard data were collected between July 7th and August 18th 2024, and the laboratory data were collected between August 18th and December 31st 2024.
Data exclusions	No data were excluded from these analyses
Reproducibility	All chemosynthetic communities were recorded in video. All analyses were conducted based on duplicate materials.
Randomization	This is not relevant to our study because no comparative experiment is applied to this study.
Blinding	This is not relevant to our study because no comparative experiment is applied to this study.

Did the study involve field work? Yes No

Field work, collection and transport

Field conditions	Water depths range from 5662m to 9570m.
Location	This study was conducted at the Kuril-Kamchatka Trench and the western Aleutian Trench (from 44.4N 150.1E to 53.1N 169.2E along trench axis)
Access & import/export	The cruise was approved by the local government.
Disturbance	No disturbance was caused to the environment.

Reporting for specific materials, systems and methods

We require information from authors about some types of materials, experimental systems and methods used in many studies. Here, indicate whether each material, system or method listed is relevant to your study. If you are not sure if a list item applies to your research, read the appropriate section before selecting a response.

Materials & experimental systems

n/a	Involved in the study <input checked="" type="checkbox"/> Antibodies <input checked="" type="checkbox"/> Eukaryotic cell lines <input checked="" type="checkbox"/> Palaeontology and archaeology <input type="checkbox"/> Animals and other organisms <input checked="" type="checkbox"/> Clinical data <input checked="" type="checkbox"/> Dual use research of concern <input checked="" type="checkbox"/> Plants
-----	--

Methods

n/a	Involved in the study <input checked="" type="checkbox"/> ChIP-seq <input checked="" type="checkbox"/> Flow cytometry <input checked="" type="checkbox"/> MRI-based neuroimaging
-----	---

Animals and other research organisms

Policy information about [studies involving animals; ARRIVE guidelines](#) recommended for reporting animal research, and [Sex and Gender in Research](#)

Laboratory animals

This study did not involve laboratory animals.

Wild animals

We have collected a small amount of tubeworms and bivalves from the field for taxonomic and molecular studies.

Reporting on sex

Sex was not considered in this study.

Field-collected samples

No incubation work in laboratory was conducted with field collected samples.

Ethics oversight

Only low invertebrates are involved in this study.

Note that full information on the approval of the study protocol must also be provided in the manuscript.

Plants

Seed stocks

No plant specimen were collected in this study.

Novel plant genotypes

No novel plant genotypes.

Authentication

No authentication procedures are needed.